Generation and Initial Evolution of a Mode Water θ-S Anomaly

Gregory C. Johnson[1,2]

Submitted 16 May 2005

to the

Journal of Physical Oceanography

Revised 15 September 2005

[1] NOAA/Pacific Marine Environmental Laboratory, 7600 Sand Point Way, Bldg. 3, Seattle Washington 98115-6349, U.S.A

[2] Corresponding author. Tel.: +1-206-526-6806; fax: +1-206-526-6744, E-mail address: gregory.c.johnson@noaa.gov (G. C. Johnson).

Abstract

Generation and evolution of an isopycnal potential temperature-salinity (θ-S), or spiciness, anomaly is studied around 20-23°S, 110°W in the austral winter of 2004. Two profiling CTD floats deployed in the region in January 2004 provide the observations. The anomaly (defined as relative to water properties of the preceding summer) is quite large (initially about 0.35 in S and about 0.9°C in θ). It is associated with the winter ventilation of a thick, low potential vorticity layer known as South Pacific Eastern Subtropical Mode Water. Regional lateral θ and S distributions at the surface predispose the ocean to formation of this water mass, and allow significant anomalies to be generated there with relative ease. The water mass is potentially important for climate in that, after northwestward advection in the South Equatorial Current, it contributes to the Equatorial Undercurrent and eventually resurfaces in the cold tongue of the eastern equatorial Pacific. The anomaly studied is strong enough to predispose a portion of the water column to salt fingering, increasing vertical mixing. While lateral processes are doubtless important in evolution of the anomaly, the vertical mixing appears sufficiently vigorous to reduce it significantly within six months after its formation by spreading it to denser horizons through diapycnal fluxes. By that time the anomaly is most likely sufficiently diffuse so that subsequent evolution from diapycnal fluxes is significantly reduced as it makes its way toward the equator.

1. Introduction

Variation in the potential temperature-salinity (θ-S) relationship at a fixed density (Veronis 1972) is often referred to as spiciness (Munk 1981), since water on an isopycnal can be either relatively cold and fresh, or hot and salty. Spreading of subducted water property anomalies, especially isopycnal θ-S anomalies, to a remote location where they can resurface and affect air-sea interaction is one hypothetical teleconnection mechanism for climate variability. This mechanism was proposed for anomalies subducted in the subtropical Pacific Ocean, advected westward and equatorward by the general circulation to feed the Equatorial Undercurrent, and then carried eastward to upwell in the cold tongue of the eastern equatorial Pacific, where they might influence SST and the El Niño Southern Oscillation (Gu and Philander 1997). Two possible routes for advection of these anomalies exist in each hemisphere of the Pacific, a direct route generally westward and equatorward in the ocean interior for waters subducted sufficiently eastward and equatorward, or similar flow to the western boundary followed by equatorward advection in the western boundary currents.

Subsequent to the advancement of this hypothesis, substantial analysis was completed on tropical-subtropical connections in all three major ocean basins (see Schott et al. 2004 for a review). Much of this work suggests that variations in the strength of the ocean circulation, rather than variations in the water properties carried by the circulation, are more likely to be related to variations in the equatorial surface temperature.

Nonetheless, there are a few analyses of numerical modeling results (Schneider 2000; Yeager and Large 2004) that suggest that isopycnal θ-S variations are preferentially generated by anomalous advection or subducted in certain locations. Furthermore, some of these θ-S anomalies, whether generated in the tropics or subducted in the subtropics, could make their way

to the equator, somewhat diminished in magnitude by mixing processes along their route, and subsequently emerge at the surface through equatorial upwelling to influence the atmosphere. Model analysis (Yeager and Large 2004) suggests that the subducted anomalies, both in the subtropics and other parts of the world ocean, appear downstream of regions with a near-surface unstable vertical salinity gradient.

Mode waters are nearly vertically homogenous water masses found over a relatively large geographical area (Hanawa and Talley 2001), so-called because they cause a θ-S mode in bivariate volumetric water mass censuses. Mode waters are also associated with pycnostads, regions of reduced vertical density gradient. Interestingly, locations from the model with large θ-S variability on isopycnals (Yeager and Large 2004) are coincident with many mode water locations (Hanawa and Talley 2001). This coincidence may be expected because the destabilizing vertical salinity gradient in these regions of large variability will tend to reduce the vertical density gradient there, favoring mode water creation. In addition, where salinity is destabilizing, variations in θ-S are amplified on isopycnals. This amplification arises because the θ-S curves in these regions are closer to being parallel to isopycnals, since the vertical gradients of these two water properties there largely compensate in their effects on density.

One study of variations in the properties of the Eighteen Degree Water, the subtropical mode water found in the western North Atlantic Ocean (Jenkins 1982) demonstrated that high wintertime latent heat flux from ocean to atmosphere is well correlated with increased mixed layer S (and therefore θ) on isopycnals, reduced vertical stratification, and increased oxygen levels within mode waters on interannual and longer time scales. This analysis observationally linked increased mode water production with θ-S anomalies on isopycnals in one location, and

proposed a simple model for anomalously strong wintertime latent heat loss to increase S and θ on isopycnals within mode water.

The South Pacific Eastern Subtropical Mode Water (SPESTMW; Hanawa and Talley 2001) exhibits a large (around 70° longitude by 20° latitude) geographical distribution, a substantial (9×10^6 m^3 s^{-1}) formation rate, a direct route to the equator, and an unstable vertical salinity gradient favoring isopycnal θ-S anomalies (Wong and Johnson 2003). These characteristics allow SPESTMW θ-S variations to reach the equator in at least one numerical model (Yeager and Large 2004). Observational evidence also exists for substantial θ-S variations around the density of the salinity maximum (just above the SPESTMW) in the low latitude western Pacific (Kessler 1999). In addition, the upper ocean of the Subtropical South Pacific, like most of the other subtropical ocean basins (with the exception of the North Pacific subtropics), appears to be trending generally saltier with time over the last several decades (Boyer et al. 2005). Such subtropical salinification is a possible fingerprint of an increased hydrological cycle magnitude associated with a warming climate (Wong et al. 1999).

However, there are few data at the formation region of SPESTMW to show the creation of isopycnal θ-S anomalies. Yeager and Large (2004, their Fig. 10) display a single CTD profile taken near 15°S, 88°W during September (austral late winter) 1967 to argue that the late winter mixing has resulted in a 40-m interval just below the mixed layer where the destabilizing vertical salinity gradient nearly exceeds the stabilizing vertical temperature gradient in terms of their relative contributions to the vertical density gradient. The existence of such conditions over this large a depth range would be remarkable, since a double-diffusive process, salt fingering, tends to reduce destabilizing salinity gradients over time, generally limiting them no more than about half the magnitude of stabilizing temperature gradients in terms of their relative contributions to

the vertical density gradient (Schmitt 1981). However, close inspection of the data reveals that they were linearly interpolated between relatively coarse vertical intervals (as much as 40 m), so the vertical structure of the density ratio is not as well resolved as the closer spacing of the interpolated profile would suggest.

The Argo Project (Roemmich et al. 2004) is deploying profiling CTD floats globally, including some in the SPESTMW formation region. First this region is put into context through discussion of the compensation of later-winter horizontal temperature gradients by salinity gradients, and the relation of the compensation to observed mode water formation regions. Then time series of CTD data from a few floats are presented to illustrate the SPESTMW ventilation process. The data show that in the austral winter of 2004 a significant isopycnal θ-S anomaly was produced in SPESTMW relative to prior conditions. This sort of feature is suggested to occur at the end of strongly ventilated winters by numerical model results in the SPESTMW (Yeager and Large 2004), just below the S maximum. The generation and evolution of this patch of anomalously warm and salty water associated with a strongly destabilizing vertical salinity gradient is discussed, including the likely role of salt fingering in the subsequent evolution and decay of the anomaly. Finally, it is noted that the data suggest that spring restratification in this region may be accompanied by differential lateral advection within the SPESTMW.

2. Data and analysis methods

Data are taken from two Argo Project floats (WMO #4900451 and WMO #4900454), both Webb Research Corporation APEX 260 floats equipped with Sea-Bird Electronics Incorporated model SBE-41 CTDs. The floats are programmed to drift at 1000 dbar for 10 days, then sink in less than 6 hours to 2000 dbar and upon reaching that pressure, immediately rise to

the surface over about 6 hours taking 71 measurements of salinity (S), temperature (T), and pressure (P) at pre-selected pressures. Sample intervals for these floats start at 100-dbar intervals around 2000 dbar and logarithmically reduce to 8 dbar by 160 dbar, then remain at that resolution to the surface. Once the floats have transmitted their data while at the surface, they again sink to 1000 dbar, to start the cycle again. For WMO #4900451 the first profile was taken on 18 January 2004, and the last analyzed was on 16 September 2005. For WMO #4900454 only profiles from 18 January 2004 through 12 July 2005 were analyzed, because of a problem with the float pressure sensor after the latter date.

Since both floats do not move far with respect to large-scale water mass property distributions (less than a degree in latitude and three degrees in longitude) over the time analyzed, the data from each are treated as time series. The 10-day time intervals appear sufficient to document the seasonal evolution of water properties. The floats do not move much because they spend most of their time at 1000 dbar, where absolute mean velocities are quite weak (<0.01 m s^{-1}), and eddy diffusivities relatively low (<1000 m^2 s^{-1}) regionally (Davis 2005). However, within the upper 400 dbar, the portion of the water column analyzed here, locally the subtropical gyre exhibits a strong westward geostrophic flow with some equatorward component (Reid 1997), the South Equatorial Current.

The manufacturer quotes the CTD accuracies for T, S, and P as 0.002°C, 0.005 PSS-78, and 2.4 dbar, respectively. Comparisons of deep float θ-S relations to historical data (e.g. Wong et al. 2003) indicate that one of the floats (4900451) may be reading about 0.003 fresh of climatology, and the other (4900454) about 0.014 fresh, but historical data are sufficiently sparse in the region that no corrections are made to the reported data here.

Potential density anomaly $\sigma_\theta = \rho - 1000$ kg m^{-3} and θ referenced to the surface are calculated for each data point, where ρ is the potential density. The thermal expansion coefficient, $\alpha = -\rho^{-1}(\partial\rho/\partial\theta)$, and the haline contraction coefficient, $\beta = \rho^{-1}(\partial\rho/\partial S)$, are also calculated to measure the effects of variations in θ and S. First difference estimates of buoyancy frequency squared, $N^2 = -g/\rho(\partial\rho/\partial z)$, and planetary potential vorticity, $Q = f{\cdot}N^2/g$, are made to quantify the stratification, where g is the gravitational acceleration and f is the Coriolis parameter. Finally, θ_z and S_z are estimated by first differences, and the vertical Turner angle, $Tu(z) = \arctan[(\alpha{\cdot}\theta_z)/(\beta{\cdot}S_z)]$, (Ruddick 1983) is calculated to quantify the relative contributions of θ_z and S_z to N^2. The density ratio, $R_\rho = [(\alpha{\cdot}\theta_z)/(\beta{\cdot}S_z)] = -\tan[Tu(z)+45°]$, is often used for this purpose, but has the disadvantage of singular values in the absence of a vertical salinity gradient.

For convenience, aspects of Tu are briefly reviewed (see Ruddick 1983 for more detail). Tu quantifies the contribution of the temperature gradient versus that of the salinity gradient on the density gradient in any given direction. For Tu = 0° ($R_\rho = -1$), temperature and salinity gradients contribute equally to the density gradient. Moving from 0° toward positive angles, the salinity gradient makes a smaller and smaller contribution to the density gradient, and at 45° ($R_\rho = -\infty$) the salinity gradient vanishes. From there, the salinity gradient changes sign and begins to work against the effect of the temperature gradient on the density gradient, until by 90° ($R_\rho = 1$) the salinity gradient completely compensates the temperature gradient. For Tu > 90° the salinity gradient overwhelms the temperature gradient, reversing the density gradient (and making it gravitationally unstable in the vertical). Moving from Tu = 0° toward negative angles, the temperature gradient makes a smaller and smaller contribution to the density gradient, and at Tu = –45° ($R_\rho = 0$) the temperature gradient vanishes. From there, the temperature gradient begins

to work against the salinity gradient, until by Tu = –90° (R_ρ = 1) it completely compensates for the stabilizing effect of the vertical salinity gradient. For Tu(z) < –90° the temperature gradient overwhelms the salinity gradient, reversing the density gradient (and making it gravitationally unstable in the vertical).

The float scalar quantities are smoothed and mapped to a regular time-pressure grid with a lowess filter (Cleveland and Devlin 1988) using a one-month time scale and a 25-dbar vertical scale. For the vertical derivative quantities estimated from first differences, the same time scale is used, but the vertical scale is doubled to reduce the noise in those fields. This 50-dbar scale for smoothing of vertical derivative quantities is a conservative choice, which may damp the magnitudes of these quantities on smaller vertical scales. Filtering of N^2 and Tu(z) is accomplished by constructing a complex vector using N^2 for the amplitude and Tu(z) for the phase, filtering the vector, and then recovering the low-passed N^2 and Tu(z) from the amplitude and phase of the filtered vector. This procedure deemphasizes estimates where N^2 is small and Tu(z) is likely to be noisy.

In addition, climatological θ and S fields from the World Ocean Atlas 2001 (Stephens et al. 2002; Boyer et al. 2002) are analyzed to assess their relative effects on horizontal density gradients. Seasonal averages of surface data from the winter months (Jan.–Mar. in the Northern Hemisphere and Jul.–Sep. in the Southern Hemisphere) are used as a compromise between the desire for spatially smooth fields and analysis during the season of maximum surface density. Surface density ρ is calculated from θ and S, as are α and β. The lateral gradients of all three quantities are estimated from centered differences of the 1° × 1° fields but no other filtering is applied. These gradients all have different orientations at a given point, so to quantify the

relative contributions of $\rho\alpha\nabla\theta$ and $\rho\beta\nabla S$ to $\nabla\rho$ using a scalar quantity such as Turner angle, a somewhat arbitrary choice must be made on the direction in which to make the computation.

The equatorward direction of the temperature gradient in each hemisphere is the most prominent and consistent feature of the three gradient fields. This characteristic of the large-scale surface fields motivates the formulation of the horizontal Turner angle, $Tu(\mathbf{x}) = \arctan[(\alpha\nabla\theta\cdot\nabla\theta)/(\beta\nabla S\cdot\nabla\theta)]$ used here. This particular formulation is oriented along the direction of the local surface temperature gradient. It quantifies how the projection of the horizontal salinity gradient onto the direction of the horizontal temperature gradient acts to increase or decrease the horizontal density gradient in that direction. Other choices might be oriented along the direction of the surface density gradient, or even the surface salinity gradient.

3. Large-scale context

Several locations where the horizontal salinity gradient acts to significantly counteract, and in localized regions even reverse, the effects of the horizontal temperature gradient over large spatial scales, are revealed by large positive $Tu(\mathbf{x})$ at the surface for the winter season (Fig. 1, shaded regions). Such compensation has been shown to be prominent on Rossby radius (order 10-km) scales (Rudnick and Martin 2004), especially when vertical mixing is strong (such as in the winter). The locations of large $Tu(\mathbf{x})$ on the larger scale are mostly coincident with locations where vertical salinity gradients in the upper 200 m of the water column tend to be destabilizing (Yeager and Large 2004, their Fig. 15), and where isopycnal θ-S variations are subducted in their numerical model run. In addition, the lateral density gradient is reduced in these regions, as evinced by the increased distance between potential isopycnals in these locations (Fig. 1, solid lines) in comparison with the surrounding regions. This reduction in

lateral density gradients is largely owing to the compensating effects of the lateral θ and S gradients in these regions.

Finally, these locations where surface salinity gradients tend to compensate the contribution of the surface temperature gradient to the surface density gradient are broadly associated with many of the mode waters found to date in the World Ocean (Hanawa and Talley 2001, their Plate 5.4.3). Since these regions have relatively weak lateral density gradients owing to the surface salinity distribution, perhaps it is not surprising that mode waters are formed there. Similarly, it is also not surprising that variations in surface forcing in these regions can result in large θ-S anomalies on isopycnals, since the two fields are in close compensatory balance. The strong winter mixing, mode water formation, horizontal density compensation in the mixed layer, and large θ-S anomalies may all be related.

As mentioned before, the largest and strongest region of high Tu(**x**) in the subtropics (Fig. 1) is found in the Southeast Pacific Ocean, the formation region for SPESTMW (Wong et al. 2003; Hanawa and Talley 2001). Next Argo Project profiling float CTD data recently collected in the region are used to analyze the generation and initial evolution of a θ-S anomaly within the SPESTWM.

4. θ-S anomaly generation and evolution

The two floats analyzed have remained in the same region relative to large-scale water mass properties since they were deployed in January 2004 (Fig. 2). Argo float WMO #4900451 was deployed at 23.0°S, 109.6°W, and remained in a region bounded by 23.4°S and 22.5°S in latitude and 111.3°W and 109.6°W in longitude during the time period of the analysis. The float is located well within the SPESTMW formation region (Wong and Johnson 2003). Argo float

WMO #4900454 was deployed at the same time but slightly to the north and west at 19.9°S, 111.1°W, and remained in a region bounded by 20.3°S and 19.2°S in latitude and 114.0°W and 111.1°W in longitude during the study period. This float is near the northeastern boundary of the SPESTMW formation region. Both floats report CTD profiles every 10.6 days

Many of the properties of SPESTMW have been previously described, so the focus here is on the seasonal water property variations. Potential density anomaly, σ_θ, and potential vorticity, Q, illuminate the mode water ventilation. Select θ-S diagrams and an isopycnal S anomaly help to quantify spiciness associated with that ventilation. Since anomalies are defined on isopycnals in this study, θ and S anomalies are closely related through the equation of state for seawater, so the redundant θ anomalies are not presented here. Vertical Turner angle Tu(z) emphasizes the relations among spiciness, stratification, and salt fingering.

The θ-S curves (Fig. 3) of data from three profiles of the northern float (4900454) provide a compact preview of the θ-S anomaly generation and evolution. Around March 2004 (austral fall) the θ-S curve is typical of central waters, with salinity and temperature increasing with decreasing density, so that temperature is stabilizing and salinity destabilizing (Schmitt 1981). By October 2004 (early spring), when the mixed layer is at its deepest and densest, the θ-S curve in the upper part of the water column is pulled toward warmer and saltier values on isopycnals, but this effect is limited to $\sigma_\theta < 25.2$ kg m^{-3}. As the θ-S curve is shifted saltier by winter evaporation, it increasingly parallels isopycnals because salinity becomes increasingly destabilizing, providing necessary conditions for intense salt fingering. By March 2005, the θ-S curve has evolved with fresher water found in the recently developed seasonal pycnocline ($\sigma_\theta <$ 25 kg m^{-3}). The largest θ-S anomaly at $\sigma_\theta = 25.0$ kg m^{-3} has moderated considerably. In addition, postive θ-S anomalies relative to the previous year now exist for $\sigma_\theta \leq 25.4$ kg m^{-3}, well

below the winter mixed layer density. Diapycnal mixing owing to salt fingering has worked to restabilize the water column, moving the θ-S curve away from parallel with isopycnals, by spreading the θ-S anomaly down through more of the water column. This stabilization of the water column through rotation of the θ-S curve is characteristic of salt fingering, as opposed to other turbulent processes (Schmitt 1981; 1990).

Time-pressure sections of potential vorticity, Q, for both floats, overlain by σ_θ (Fig. 4), show the mixed layer becoming steadily deeper and denser from austral early fall (March 2004) through early spring (October 2004), and then shoaling very rapidly at the onset of seasonal restratification. The maximum mixed layer pressure, as determined by where σ_θ exceeds the surface value by 0.1 kg m^{-3}, ranges from about 25 to 50 dbar at the shallowest in early fall to about 200 or 150 dbar in early spring, depending on the float. The mixed layer has $\sigma_\theta < 24.3$ kg m^{-3} in early fall 2004, increasing to $\sigma_\theta > 25.1$ kg m^{-3} or $\sigma_\theta > 24.9$ kg m^{-3} by early spring 2004, depending on the float.

The Wong and Johnson (2003) definition of SPESTMW ($|Q| < 300 \times 10^{-12}$ m^{-1} s^{-1}) is met in these data for roughly 24.9 kg $m^{-3} < \sigma_\theta < 25.5$ kg m^{-3} during most of the year (Fig. 4), within about ±0.1 kg m^{-3} depending on the float. Below the denser surface, |Q| increases to around 400×10^{-12} m^{-1} s^{-1} in the permanent pycnocline. Above the lighter surfaces, |Q| has even larger values within the seasonal pycnocline. As the base of the mixed layer deepens in the winter, |Q| there exceeds the SPESTMW definition within the SPESTMW density range while that range is being directly ventilated. Note that Q need not be conserved in the presence of surface forcing. However, this exception at the mixed-layer base quickly vanishes when spring restratification commences. The SPESTMW is thicker with Q values that are closer to zero after the austral winter 2004 ventilation period than in the previous year. Thus, although winter 2003 ventilation

was not observed with the floats, comparison of conditions after winter 2003 relative to conditions after winter 2004 suggests that winter 2004 was more effective locally than winter 2003 in ventilating the mode water.

S anomalies for each float are defined relative to the σ_θ-S curve for the profile from each float in the first half of 2004 that samples the lightest surface waters (Fig. 5). These profiles are taken in March and April 2004, in austral late summer or early fall. The effect of latent cooling on salinity on seasonally ventilated isopycnals (Jenkins 1982) is revealed by these S (and therefore θ) anomalies on isopycnals. Well below the mixed layer (for $\sigma_\theta > 25.5$ kg m^{-3}) S anomalies are not much above 0.05 in magnitude. However, in the mixed layer S anomalies generally increase through the fall and winter 2004 into October (early spring) to a peak of about 0.35 before the onset of spring stratification. Of course a S anomaly on an isopycnal is always associated with a θ anomaly. In this case the maximum θ anomaly is about 0.9°C.

These θ-S anomalies presumably arise in part from the strong evaporation associated with wintertime latent cooling and the increased southeasterly trade winds during the fall and winter. It may seem counterintuitive that strong latent heat flux out of the ocean in the winter would result in a warm (although salty) anomaly. However, it is important to remember that these anomalies are defined on isopycnals, so with salinity increasing due to the evaporation associated with the latent heat flux, temperature on isopycnals must rise with the salinity. The maximum mixed layer density should still be relatively high (and minimum mixed layer temperature low) in winters with strong latent heat loss from the ocean. The increased S anomaly in spring 2004 relative to the previous early fall (see also Fig. 3) is consistent with thicker SPESTMW with lower Q values, as both tend to result from stronger ventilation of mode waters (e.g., Jenkins 1982).

At the onset of spring stratification, the maximum θ-S anomaly is found in the subsurface, within the SPESTMW, where it is presumably advected westward and equatorward within the South Equatorial Current. Thereafter the anomaly generally decays at the maximum, which is found near the maximum mixed layer density for the winter. However, there is another subtle effect, which is the slow shift of the θ-S anomaly to denser isopycnals as it decays. This shift can be seen by comparing the March 2005 θ-S curve to that from October 2004 in Fig. 3 for $25.1 < \sigma_\theta < 25.5$ kg m^3) or by noting the overall tendency of positive θ-S anomalies toward higher densities from around September 2004 through at least June 2005 in Fig. 5. This effect is characteristic of elevated diapycnal salinity fluxes (with respect to temperature fluxes) from salt fingering activity (Schmitt 1981; 1990), as discussed below.

As mentioned above, the vertical Turner angle, Tu(z), is one way to quantify the slope of the θ-S curve (Fig. 6). Here only Turner angles at and above 71.6° ($R_\rho < 2$) are contoured and highlighted with shading. This value is about typical of central waters where salt fingering is favored. For Tu(z) > 77° ($R_\rho < 1.6$) , salt fingering is quite active in the ocean (Schmitt 1981; St Laurent and Schmitt 1999). Early in the time-series, peak values of Tu(z) > 74.1°, sometimes even Tu(z) > 75.5°, are present near σ_θ = 25.3 or 25.4 kg m^{-3}, right in the middle of the SPESTMW. As the mixed layer deepens, and θ-S anomalies increase within and just below the mixed layer, at the base of the mixed layer Tu(z) > 77°, so these anomalies are forcing significant increases in double diffusion. Note that within the mixed layer the vertical salinity and temperature gradients are minimal, so Tu(z) is not well defined. In the following months, Tu(z) under the maximum θ-S anomaly decays as the anomaly decays, and maximum values sampled by each float nearly reach the lower pre-ventilation levels over the time period sampled. This rapid reduction in high Turner angle values after their introduction by surface forcing is

strongly suggestive of the role of double-diffusive processes, as opposed to other turbulent mixing processes (Schmitt 1981; 1990).

Increasingly high Tu (for $71° < Tu < 90°$), or equivalently increasingly low density ratios (for $2.05 > R_\rho > 1$), appear to be associated with increased salt fingering and in turn with increased diapycnal diffusion and preferential diffusion of salinity with respect to temperature (St. Laurent and Schmitt 1999). Data from this study (their Fig. 16) suggests this relation. These data are exploited here to explore the role of salt fingering in the evolution of the θ-S anomaly. To accomplish this goal the ad-hoc form of the Yeager and Large (2004, their eq. B1) parameterization of diapycnal salt diffusion, K_s, is adopted and fit solely to the St. Laurent and Schmitt (1999, their Fig. 16) data of vertical diffusion estimates for salinity as a function of density ratio to obtain $K_s(R_\rho) = 2.4 \times 10^{-4}\ m^2\ s^{-1}\{1 - [R_\rho - 1]/[2.05 - 1]\}^3 + 0.1 \times 10^{-4}\ m^2\ s^{-1}$ for $2.05 > R_\rho > 1$ ($71° < Tu < 90°$), assuming $K_s = 0.1 \times 10^{-4}\ m^2\ s^{-1}$ elsewhere. This equation says that for this range of R_ρ (and Tu), K_s steadily increases above background level as R_ρ decreases (or Tu increases). This parameterization is only qualitative, as its functional form is ad-hoc, and the uncertainties of the data used to estimate coefficients for the function are large.

Nonetheless this parameterization can be applied to the float profile data (Fig. 7) to produce qualitative estimates of the rates of salinity change due to double diffusive diapycnal fluxes using $\partial S/\partial t = \partial(K_s \partial S/\partial z)/\partial z$, where t is time. This calculation shows a positive rate of a few tenths (PSS-78) per year below the deepening winter mixed layer, with similar negative rates (although not as certain because of very low N^2 in the mixed layer) just above, near the base of the mixed layer. Rates assuming a constant typical background diapycnal diffusivity of $K_s = K_\theta = 1.5 \times 10^{-5}\ m^2\ s^{-1}$ (Gregg, 1998) would be much smaller than those estimated using the salt fingering diapycnal diffusivity parameterization, and the dipole less pronounced. The salinity

anomaly growth below the mixed layer during this period (Fig. 5) is likely due to this diapycnal double diffusive flux. After the onset of spring restratification, the vertical dipole in $\partial S/\partial t$ continues within the deeper portions of the S anomaly. Thus double diffusion continues to affect downward diapycnal flux of the θ-S anomalies after the onset of spring restratification. These elevated diapycnal salt (and to a lesser extent temperature) fluxes work to moderate the θ-S anomaly by spreading it down into the permanent pycnocline. The inflection point between negative and positive $\partial S/\partial t$ generally shifts to increasing densities with time as the anomaly moves downward. As these double-diffusive fluxes work, they also tend to decrease the destabilizing salinity gradient, and $\partial S/\partial t$ gradually decreases to about 0.1 Yr^{-1} as a result of the downward spreading of the anomaly. The modification time scale for these anomalies starts out at about a year (an ~0.3 PSS-78 anomaly worked on by $\partial S/\partial t \sim 0.3$ Yr^{-1}), but increases rapidly to about 3 years or more as double diffusion slows and the fluxes decrease.

The effects of this diapycnal mixing can be seen in the S anomalies (Fig. 5), and the θ-S curves (Fig. 3). The maximum S (and therefore θ) anomaly is found at the height of winter ventilation. These anomalies within the locally ventilated portion of the SPESTMW decay with time after ventilation of the mode water is capped off by the commencement of restratification, while on underlying denser isopycnal surfaces, anomalies build with time.

The time-evolution of observed salinities compare favorably with those simply modeled by time integrating the $\partial S/\partial t$ (from the fields estimated above) along $\sigma_\theta = 25.35$ kg m^{-3} (Fig. 8). This isopycnal calculation is an approximate one, because double diffusion is a diapycnal process. Here the integration constant for the modeled salts has been picked to give the best agreement with observations. Comparisons around this isopycnal are better than most, likely because it is light enough to be located within the region of strong fluxes for some of the time

but somewhat denser than the maximum winter mixed layer σ_θ, keeping it below other diapycnal processes associated with a deepening mixed layer, such as mixing owing to penetrative convection or enhanced shear from inertial oscillations and internal waves. Observed values are noisier than modeled values, which is to be expected given water-mass variations in the presence of lateral advection and mixing. In the southern float (Fig 8a), the S anomaly increases starting in September 2004, both in the model and observations, when the S anomaly introduced by winter ventilation initiates diapycnal salinity flux from above. Later on, in November, as the inflection point in $\partial S/\partial t$ moves across this isopycnal, the salinity on it decreases. In the northern float (Fig. 8b) with a lighter maximum late winter mixed layer density, it takes some time after ventilation for the S anomaly to reach $\sigma_\theta = 25.35$ kg m^{-3}, likely via diapycnal fluxes, but by November 2004 both modeled and observed salts start to increase, and they appear to have begun to decrease by July 2005, the end of the period analyzed.

The qualitative agreement of these calculations is quite encouraging given the uncertainty in the diapycnal mixing parameterization. Integrations for θ on isopycnals using a double-diffusive parameterization for K_θ, the same as that used here for K_s but scaled by 8/13 (following St. Laurent and Schmitt 1999) are not shown, but give similar model-observation agreement. However, use of a constant background vertical diffusivity of $K_s = K_\theta = 1.5 \times 10^{-5}$ m^2 s^{-1}, typical of values observed in the interior ocean (Gregg 1998), as well as the central waters (Ledwell et al. 1998), results in modeled changes in S and θ (not shown) that are a few times smaller than observed changes, bolstering the suggestion that double diffusive processes may be important in the evolution of the θ-S anomaly studied here.

5. Discussion

A large positive θ-S anomaly is introduced within the SPESTMW in austral winter 2004, compared with the θ-S relation in the same location during the preceding summer. In addition, the low potential vorticity signature of the mode water is reinforced during winter ventilation. Both of these variations are likely associated with stronger than usual latent heat fluxes from ocean to atmosphere (Jenkins 1982). The anomaly at the end of the winter ventilation period is large, with isopycnal salinity anomalies initially exceeding 0.35 (and corresponding temperature anomalies exceeding 0.9°C). The anomalously warm and salty water increases the propensity of the water column for double diffusion. These processes reduce the magnitude of the anomaly at the density at which it was introduced through diapycnal fluxes to denser horizons. The magnitude of the anomaly is about half or less its original size only six months after wintertime ventilation on lighter isopycnals, but it increases on denser isopycnals, as expected. Diapyncal fluxes predicted from application of a crude parameterization of salt fingering diapycnal diffusivity strength to the observed upper ocean structure are of the correct sign and about the right order of magnitude to effect much of these changes.

This study has focused on the role of enhanced diapycnal fluxes from double diffusion in the evolution of these θ-S anomalies. However, lateral processes are also clearly important in the evolution of the SPESTMW properties. Some evidence of this assertion is that features like the isopycnal S (and θ) anomaly are somewhat irregular, waxing and waning in time after the winter ventilation, especially for the southern float (Fig. 5a). This variability must be lateral, and isopycnal fluxes doubtless work to homogenize this variability over time.

In addition, isopycnals at pressures between the surface and 200 dbar show rapid vertical excursions after the commencement of spring restratification, especially in the southern float, but also in the northern one (Fig. 4). A closer look at this restratification for the southern float (Fig.

9) shows that only 20 days after wintertime ventilation ceased, significantly denser water is found from 70–210 dbar, and lighter water from 0–70 dbar. While surface buoyancy fluxes likely account for some of the restratification from 0–70 dbar, the deeper restratification seems most likely to arise from lateral advection. One possible cause for this advection could be slumping of the mixed layer after wintertime cooling ceases. The density increase for this float is about 0.1 kg m^{-3} on average over 20 days from 70–210 dbar. Large-scale winter lateral surface density gradients are about 1×10^{-6} kg m^{-4} in the vicinity of the floats (Fig. 2). To account for this density increase by horizontally sheared advection within the SPESTMW the velocity field near 200 dbar would have to be more northwestward than that at 70 dbar by the order of 0.1 m s^{-1}. A similarly sized southeastward surface velocity relative to 70 dbar could account for some of the near-surface density decrease. Of course, these flows would likely be in geostrophic balance, since they are mostly found below the seasonal pycnocline. However, the large-scale lateral surface density gradients are too small by an order of magnitude to support this much geostrophic shear over the top 200 dbar of the water column. Adjustment of smaller scale (perhaps mesoscale) winter mixed layer water property variability during the springtime restratification may also play a role, but that process cannot be assessed here.

Model output suggests that salinity anomalies are likely to take several years to transit from the SPESTMW formation region to the equator (Yeager and Large 2004). Over that time, this study suggests that double diffusion significantly reduces the size of positive θ-S anomalies, rapidly at first, and then much more slowly as the anomaly is spread down though the water column by this mixing, making it less susceptible to double diffusion. This result would seem to call into question the effectiveness of equatorial upwelling of remotely subducted water property

anomalies (at least those favorable for double-diffusion) as a cause for modulation of equatorial sea surface temperature, as outlined in the introduction.

However, despite these mixing processes, a series of anomalous winters might allow a significant θ-S anomaly to build up in a mode water and make its way northwestward toward the equator in the South Equatorial Current, one possible explanation for observed interannual θ-S variations downstream of the SPESTMW formation region (Kessler 1999). In addition, SPESTMW is not the only source water for the Equatorial Undercurrent (Tsuchiya et al. 1989) and some of these waters, such as the denser South Pacific shallow salinity minimum formed to the southeast of the SPWESTMW, may also be susceptible to θ-S variability (Karstensen 2004).

Acknowledgments: The NOAA Office of Oceanic and Atmospheric Research and the National Ocean Partnership Program helped to support this research. The float data were collected and made freely available by the International Argo Project (a pilot program of the Global Ocean Observing System) and the national programs that contribute to it (http://www.argo.net/). Discussions with Donald Denbo, William Kessler, John Lyman, and LuAnne Thompson helped in writing the manuscript. Comments of Eric Kunze, Annie Wong, and two anonymous reviewers on the manuscript helped to improve it. This is Pacific Marine Environmental Laboratory contribution number 2806.

REFERENCES

Boyer, T. P., J. I. Antonov, S. Levitus, and R. Locarnini, 2005: Linear trends of salinity for the World Ocean, 1955–1998. *Geophys. Res. Lett.* , **32**, L01604, doi:1029:2004GL021791.

Boyer, T. P., C. Stephens, J. I. Antonov, M. E. Conkright, R. A. Locarnini, T. D. O'Brien, and H.

E. Garcia, 2002: World Ocean Atlas 2001, Volume 2: Salinity. S. Levitus, Ed., NOAA Atlas NESDIS 50, U.S. Government Printing Office, Wash. D.C., 165 pp.

Cleveland, W. S., and S. J. Devlin, 1988: Locally weighted regression: An approach to regression analysis by local fitting. *J. Amer. Stat. Assoc.*, **83**, 596–610.

Davis, R. E., 2005: Intermediate-depth circulation of the Indian and South Pacific Oceans measured by autonomous floats. *J. Phys. Oceanogr.*, **35**, 683–707.

Gregg, M. C. (1998): Estimation and geography of diapycnal mixing in the stratified ocean, in *Physical Processes in Lakes and Oceans, Coastal and Estuarine Studies*, Vol. **54**, J. Imberger, ed., American Geophysical Union, 305–338.

Gu, D., and S. G. H. Philander, 1997: Interdecadal climate fluctuations that depend on exchanges between the tropics and extratropics, *Science*, **272**, 805–808.

Hanawa, K., and L. D. Talley, 2001. Mode Waters. In *Ocean Circulation and Climate—Observing and Modelling the Global Ocean*, G. Siedler, J. Church, and J. Gould, eds., Academic Press, 373–368.

Jenkins, W. J., 1982: On the climate of a subtropical ocean gyre: Decade timescale variations in water mass renewal in the Sargasso Sea. *J. Mar. Res.*, **40**, Suppl., 265–290.

Karstensen, J., 2004: Formation of the South Pacific shallow salinity minimum: A Southern Ocean pathway to the tropical Pacific. *J. Phys. Oceanogr.*, **34**, 2398–2412.

Kessler, W. S., 1999: Interannual variability in the subsurface high-salinity tongue south of the equator at 165°E. *J. Phys. Oceanogr.*, **29**, 2038–2049.

Ledwell, J. R., A. J. Watson, and C. S. Law, 1998: Mixing of a tracer in the pycnocline. *J. Geophys. Res.*, **103**, 21,499–21,529.

Munk, W., 1981: Internal waves and small-scale processes. In *Evolution of Physical Oceanography*, B. A. Warren and C. Wunsch, eds., MIT Press, 264–291.

Reid, J. L., 1997: On the total geostrophic circulation of the Pacific Ocean: flow patterns, tracers, and transports. *Prog. Oceanogr.*, **39**, 263–352.

Ruddick, B., 1983: A practical indicator of the stability of the water column to double-diffusive activity. *Deep-Sea Res. Part A*, **30**, 1105–1107.

Rudnick, D. L., and J. P. Martin, 2002: On the horizontal density ratio in the upper ocean. *Dynam. Atmos. Oceans*, **36**, 3–21.

Schmitt, R. W., 1981. Form of the temperature-salinity relationship in the Central Water: Evidence for double-diffusive mixing. *J. Phys. Oceanogr.*, **11**, 1015–1026.

Schmitt, R. W., 1990. On the density ratio balance in the Central Water. *J. Phys. Oceanogr.*, **20**, 900–906.

Schneider, N., 2000: A decadal spiciness mode in the tropics. *Geophys. Res. Lett.*, **27**, 257–260.

Schott, F. A., J. P. McCreary, Jr., and G. C. Johnson, 2004. Shallow overturning circulations of the tropical-subtropical oceans, in *Earth's Climate: The Ocean-Atmosphere Interaction*, C. Wang, S.-P. Xie, and J. A. Carton, eds., Geophysical Monograph 147, American Geophysical Union, pp. 261–304.

St. Laurent, L., and R. W. Schmitt, 1999: The contribution of salt fingers to vertical mixing in the North Atlantic Tracer Release Experiment. *J. Phys. Oceanogr.*, **29**, 1404–1424.

Stephens, C., J. I. Antonov, T. P. Boyer, M. E. Conkright, R. A. Locarnini, T.D. O'Brien, and H.E. Garcia, 2002: World Ocean Atlas 2001, Volume 1: Temperature. S. Levitus, Ed., NOAA Atlas NESDIS 49, U.S. Government Printing Office, Wash. D.C., 167 pp.

Tsuchiya, M., R. Lukas, R. A. Fine, E. Firing, and E. Lindstrom, 1989: Source waters of the Pacific Equatorial Undercurrent. *Prog. Oceanogr.*, **23**, 101–147.

Veronis, G., 1972. On properties of seawater defined by temperature, salinity and pressure. *J. Mar. Res.*, **30**, 227–255.

Wong, A. P. S., N. L. Bindoff, and J. A. Church. 1999: Large-scale freshening of the intermediate waters in the Pacific and Indian Oceans. *Nature*, **400**, 440–443.

Wong, A. P. S., and G. C. Johnson, 2003: South Pacific Eastern Subtropical Mode Water, *J. Phys. Oceanogr.*, **33**, 1493–1509.

Wong, A. P. S., G. C. Johnson, and W. B. Owens, 2003: Delayed-mode calibration of autonomous CTD profiling float salinity data by θ-S climatology. *J. Atmos. Oceanic Technol.*, **20**, 308–318.

Yeager, S. G., and W. G. Large, 2004: Late-winter generation of spiciness on subducted isopycnals. *J. Phys. Oceanogr.*, **34**, 1528–1547.

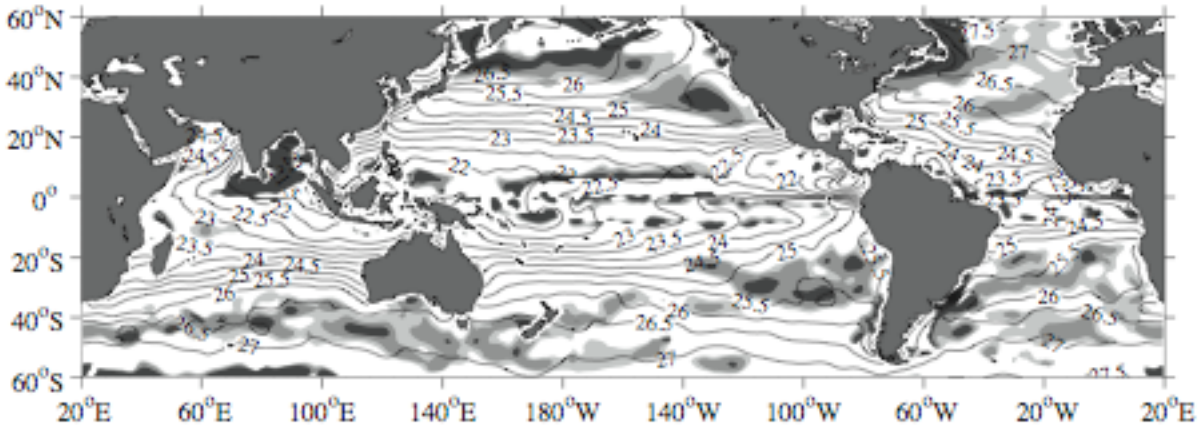

Figure 1. Horizontal Turner angle, Tu(**x**) calculated in the direction of $\nabla\theta$ (increasingly grey shaded for values above 71.6°, 78.7°, and 90° (R_ρ values below 2, 1.5, and 1, respectively). These angles shaded denote an increasingly compensating influence of $\rho\beta\nabla S$ on $\nabla\rho$ at levels 1/2, 2/3, and 1 (completely compensating), respectively, with regard to the influence of $\rho\alpha\nabla\theta$. Potential isopycnals (solid lines) are overlaid at 0.5 kg m^{-3} intervals. Seasonal winter climatological fields surface fields (Jan.–Mar. in the north and Jul.–Sep. in the south) from the World Ocean Atlas 2001 (Stephens et al. 2002; Boyer et al. 2002) are used in each hemisphere.

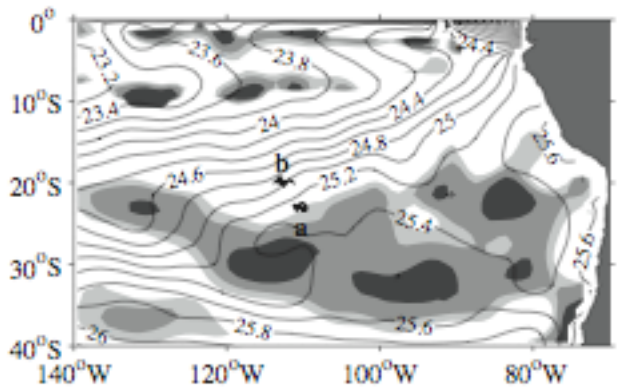

Fig. 2. Float surface positions (solid lines) of the two Argo floats analyzed in this study. The southern float (with an **a** under its trajectory) is WMO #4900451 and the northern one (with a **b** over its trajectory) is WMO #4900454. Horizontal Turner angle and potential isopycnals are the same as in Fig. 1, except that the contour interval for the latter is 0.2 kg m^{-3} here.

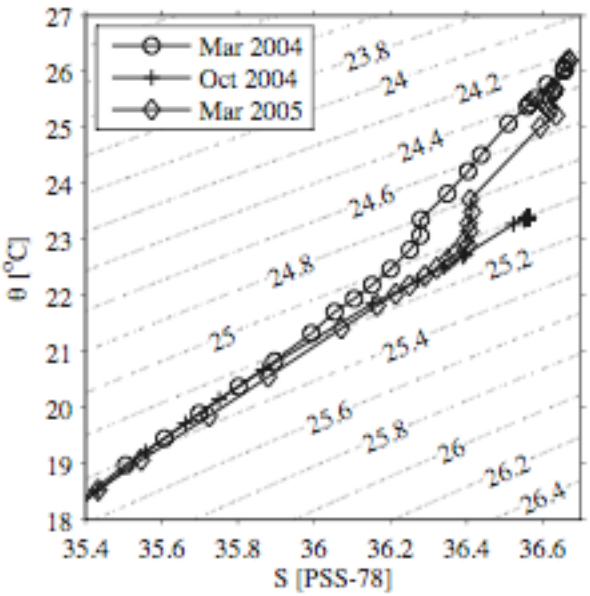

Fig. 3. Select θ-S curves for profiles from the northern float, WMO #4900454. Months and years of the profiles are denoted by the symbols at each data point taken as indicated in the legend. Potential isopycnals, σ_θ (dotted lines) are contoured at 0.2 kg m^{-3} intervals.

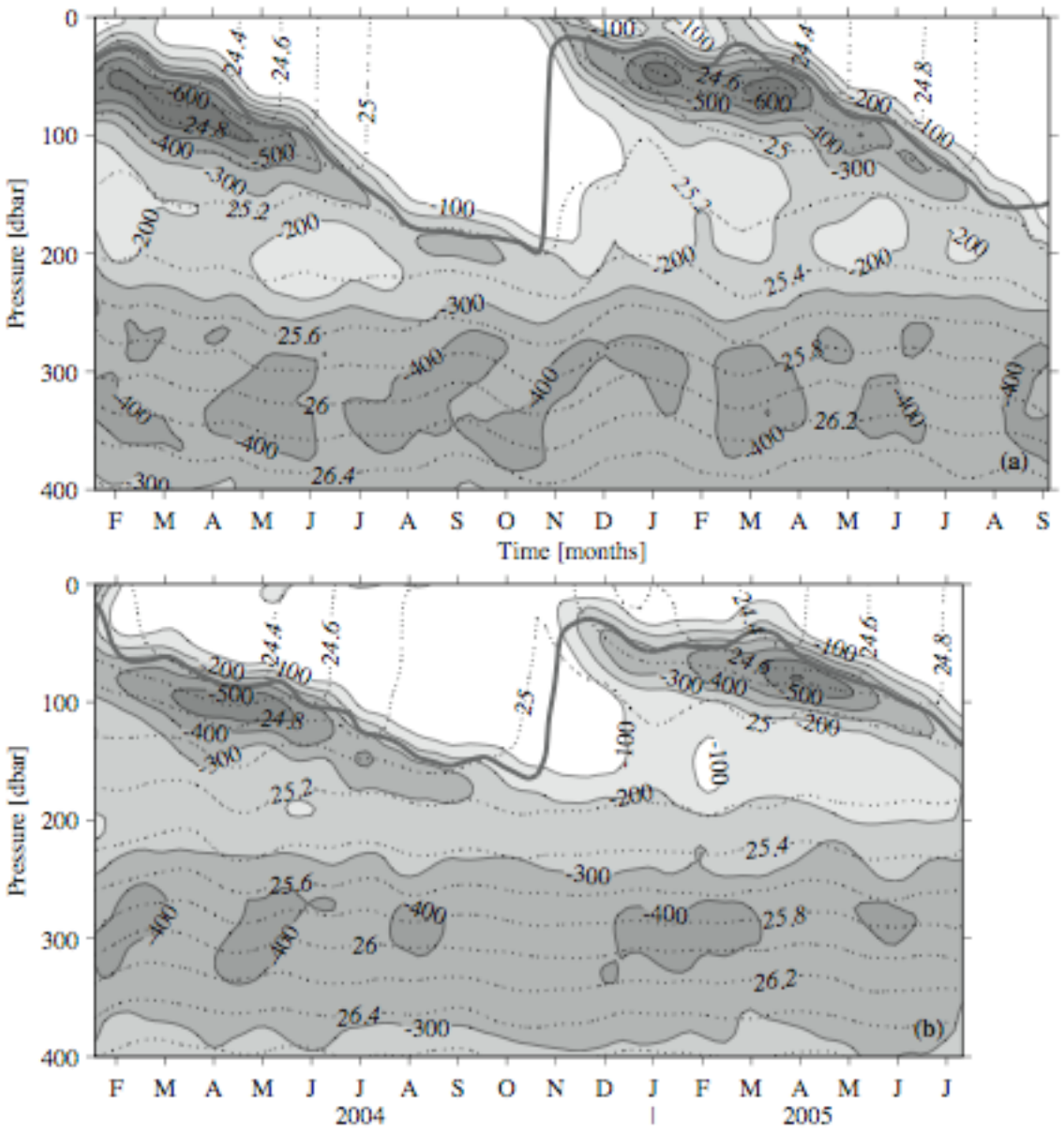

Fig. 4. Time-pressure sections of Q (10^{-12} m^{-1} s^{-1}, solid lines with increasingly negative values increasingly shaded) starting in January 2004. Also shown are σ_θ (kg m^{-3}, dotted lines with oblique contour labels) and an indicator of maximum mixed layer pressure (where σ_θ is 0.1 kg m^{-3} above the surface value, thick gray line) for (a) the southern float, WMO #4900451, and (b) the northern one, WMO #4900454. Years are noted at the bottom of the plot, separated by a vertical bar.

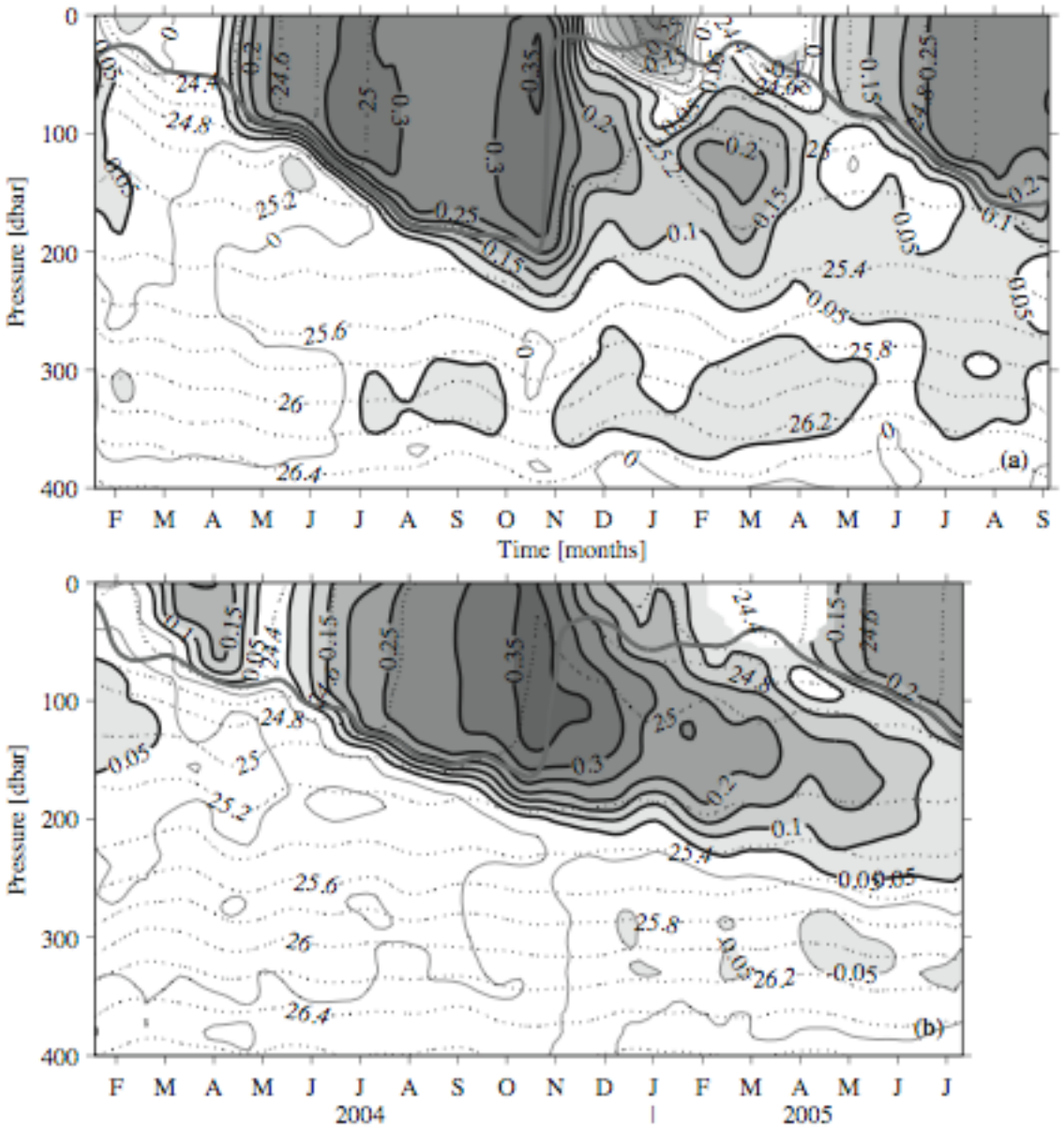

Fig. 5. Time-pressure sections of isopycnal S anomaly as defined in the text (PSS-78, with increasing magnitudes increasingly shaded, thick solid lines for positive contours, and thin solid lines for zero and negative contours). Other details follow Fig. 4.

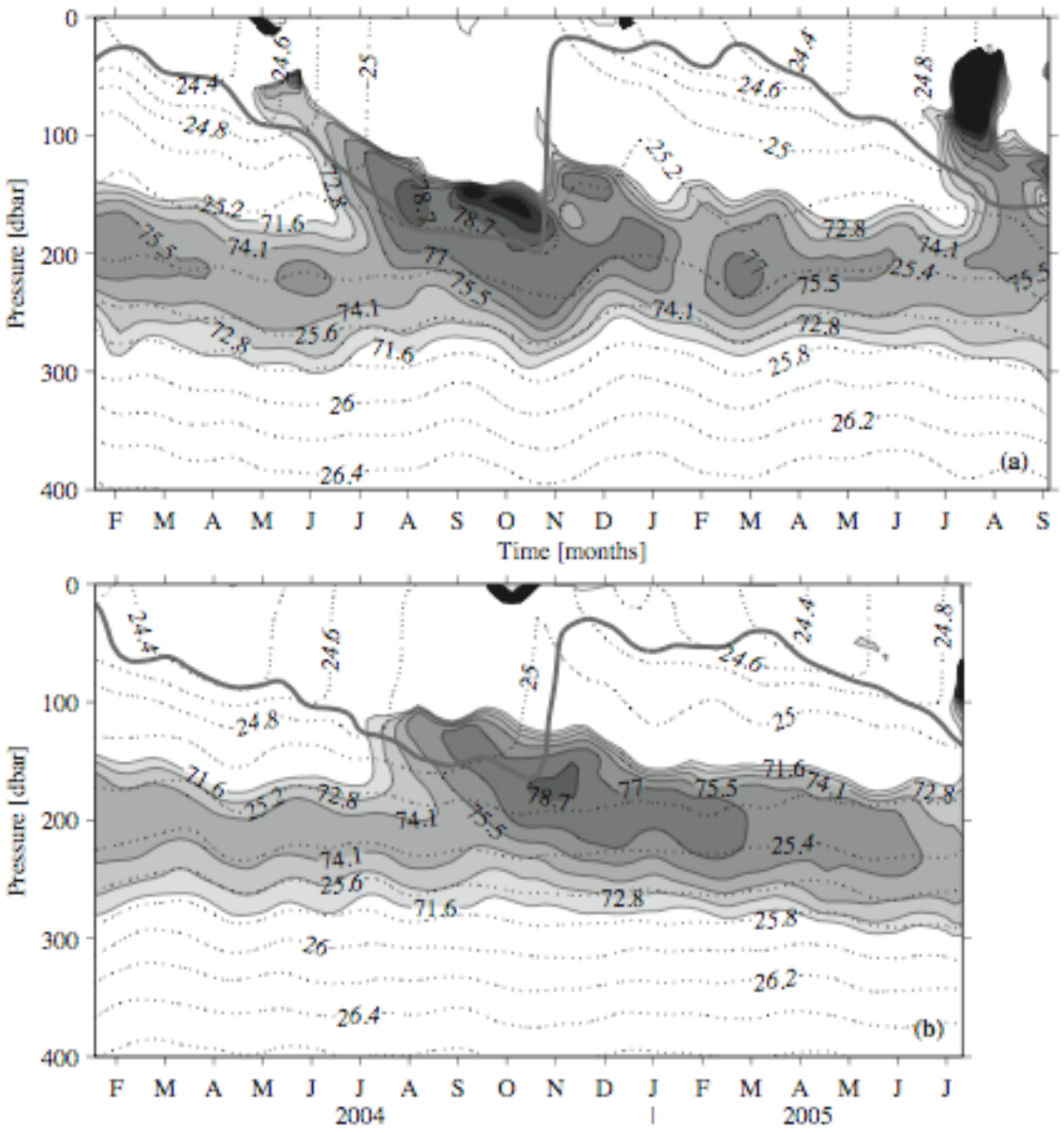

Fig. 6. Time-pressure sections of Tu(z) (°, solid lines with increasingly positive values increasingly shaded). Values of 71.6°, 72.8°, 74.1°, 75.5°, 77°, 78.7°, 80.5°, and 82.6°, 84.8°, 87.3°, and 90° correspond to R_ρ values from 2 to 1 at 0.1 intervals. Values in the mixed layer are uncertain because of the small vertical gradients there. Other details follow Fig. 4.

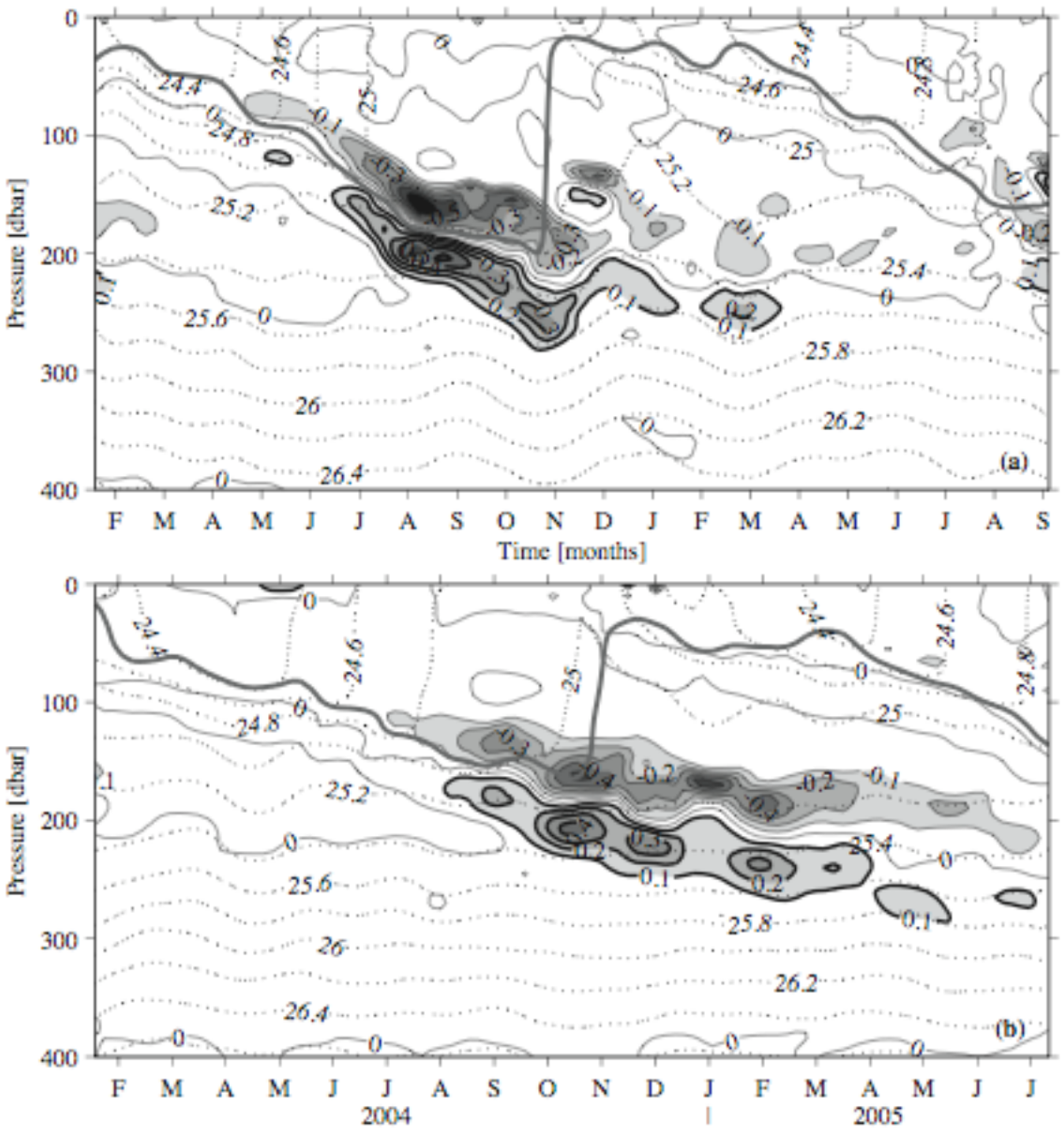

Fig. 7. Time-pressure sections of estimated diapycnal rate of salinity change (PSS-78 Yr^{-1}, with increasing magnitudes increasingly shaded, thick solid lines for positive contours, and thin solid lines for zero and negative contours) computed by application of the salt-fingering diffusion parameterization described in the text to mapped float data. Values in the mixed layer are uncertain because of the small vertical gradients there. Other details follow Fig. 4.

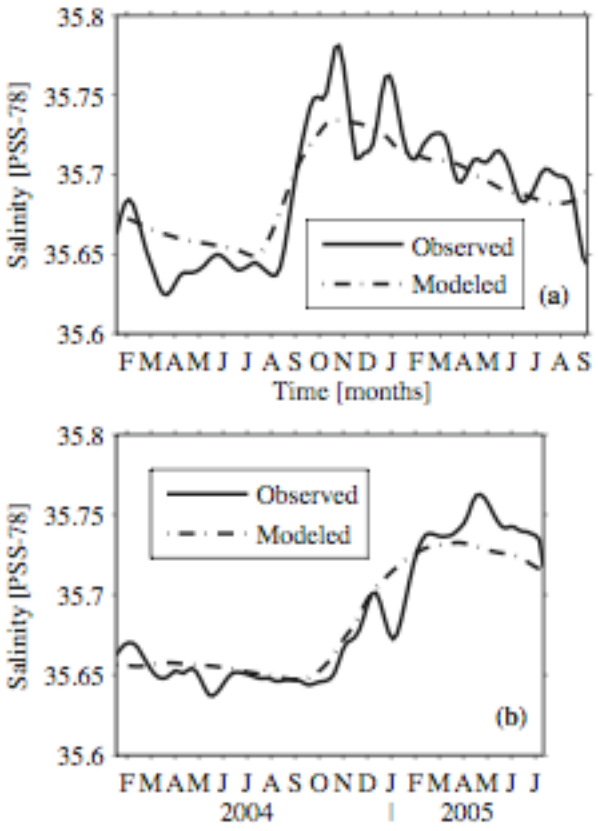

Fig. 8. Plots of observed salinity (PSS-78) vs. time on $\sigma_\theta = 25.35$ kg m^{-3} (solid line) and that modeled by time integration of the diapycnal rate of salt change (dash-dotted line) from Fig. 7 as discussed in the text for (a) the southern float, WMO #4900451, and (b) the northern one, WMO #4900454. Years are noted at the bottom of the plot, separated by a vertical bar.

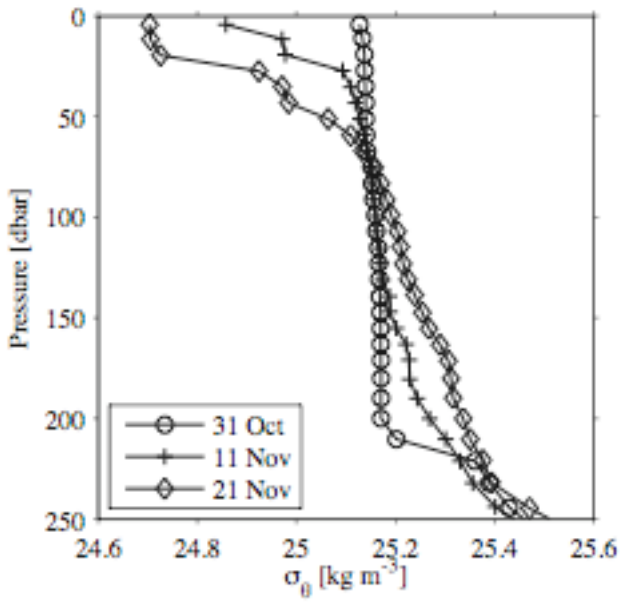

Fig. 9. Select σ_θ-P curves for profiles from the southern float, WMO #4900451. Days and months in 2004 are denoted by the symbols at each data point taken as indicated in the legend.